Metal-Enhanced Fluorescence (MEF) Due to Silver Colloids on a Planar Surface: Potential Applications of Indocyanine Green to in Vivo Imaging†

Chris D. Geddes,‡ Haishi Cao, Ignacy Gryczynski, Zygmunt Gryczynski, Jiyu Fang,§ and Joseph R. Lakowicz*

University Maryland Baltimore, Center for Fluorescence Spectroscopy, Department of Biochemistry and Molecular Biology, 725 West Lombard Street, Baltimore, Maryland 21201

Received: September 10, 2002; In Final Form: January 23, 2003

We examined the effects of metallic silver colloids on the fluorescence spectral properties of indocyanine green (ICG), which is a dye widely used for in vivo medical testing. Silver colloids from a suspension bind spontaneously to amine-coated surfaces. These colloid-coated surfaces were found to cause a 30-fold increase in the intensity of ICG, which was held close to the metal surface by adsorbed albumin. The increased intensities of ICG were also associated with decreased lifetimes and increased photostability, which are indicative of modifying the fluorophores radiative decay rate. These results suggest the use of metal colloid-enhanced ICG for applications to retinal angiography and vascular imaging and as a contrast agent for optical tomography.

Introduction

The long-wavelength tricarbocyanine dye indocyanine green (ICG, Figure 1) is widely used in medical testing. ICG appears to be essentially nontoxic and is rapidly cleared from the body.[1,2] Injected ICG is used to assess the severity of burns,[3] cardiac output,[4] and most commonly for retinal angiography.[5−9] In the later application, injected fluorescence is used to image the surface vasculature, and the longer wavelength absorption and emission of ICG is used to image the choridal vasculature behind the retina.[8,9] In the case of choridal imaging, the diagnostic value of ICG could be increased by larger intensities and decreased leakage from the vasculature.

In recent reports we have described the favorable effects of silver island films (SIFs) for increasing the intensities and photostability of fluorophores, particularly those with low quantum yields.[10−13] Such metallic surfaces interact with the fluorophores by mechanisms that can cause quenching, increased rates of excitation, and/or increased quantum yields. These effects have to be considered theoretically as part of the effort to understand surface enhanced Raman scattering (SERS).[14−18] For SERS the most commonly used system are silver island films (SIFs). These films are formed by chemical reduction of silver with direct deposition into a glass substrate,[19,20] resulting in a heterogeneous distribution of silver particles. This process is difficult to control. In contrast, preparation of colloidal suspensions of gold and silver are rather standard and easily controlled to yield a homogeneously sized suspension of spherical metal particles,[21−23] a technology used for hundreds of years for the preparation of colored glasses.[24,25] An advantage of a colloidal suspension is the possibility of injection for medical imaging.

Numerous publications have appeared on the use of SIFs for SERS[26−29] and a lesser but significant number of reports of surface enhanced fluorescence (SEF), which is also known as metal-enhanced fluorescence (MEF), using SIF substrates.[10−13,30−32] In contrast, fewer publications have appeared on SERS using silver colloids and there are only a very few reports of SEF using colloids.[33,34] These reports described fluorophores with visible excitation and emission wavelengths, and the results have been contradictory. Because the fluorophores interact with the metal through the surface plasmon resonance, and for silver the adsorption maximum is near 430 nm, we did not know if silver colloids would enhance the emission of ICG with absorption and emission maxima of 795 and 810 nm, respectively. Additionally, significantly larger effects on fluorescence are predicted for elongated silver particles than for spheres,[14] and thus it was not clear if significant enhancements could be observed using spherical colloids.

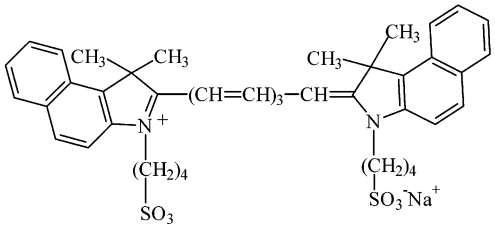

Figure 1. Chemical structure of ICG.

In the present report we studied ICG bound to human serum albumin, which is also the dominant form of ICG following intravenous injection. Albumin proteins are known to spontaneously bind to glass and silver surfaces forming essentially a complete monolayer.[34] Additionally, silver and gold colloids are known to bind spontaneously to surfaces coated with amino groups.[34,35] We used this interaction to bind silver colloids to microscope slides covered with amino groups, which in turn were coated with ICG-HSA complexes. This approach made it easy to wash away unbound colloids and proteins. Additionally, the use of colloids on surfaces circumvented the problems of the low particle concentration of a colloid suspension with a reasonable optical density of. 0.3.

† Part of the special issue "George S. Hammond & Michael Kasha Festschrift".

‡ Medical Biotechnology Center, University Maryland Biotechnology Institute, 725 West Lombard Street, Baltimore, MD 21201.

§ Center for Biomolecular Science & Engineering (Code 6900), Naval Research Laboratory, Washington, DC 20375.

10.1021/jp022040q CCC: $25.00
Published on Web 03/20/2003

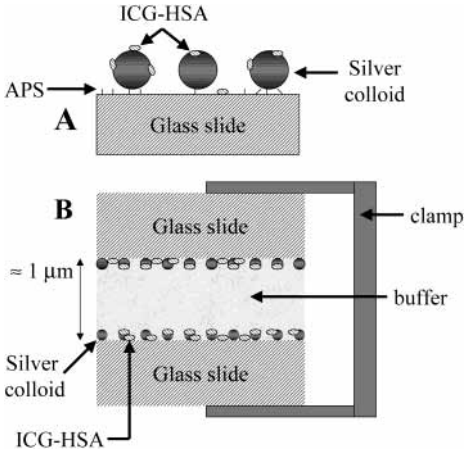

Figure 2. (A) Glass surface geometry. APS is used to functionalize the surface of the glass with amine groups that readily bind silver colloids. (B) Sample geometry.

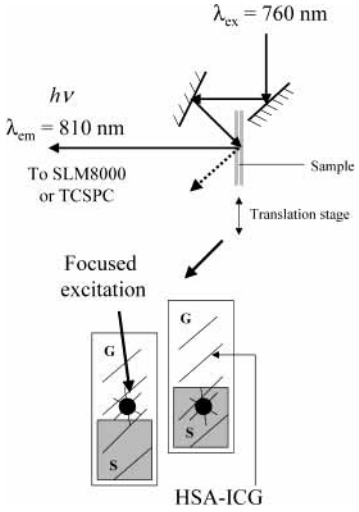

Figure 3. Experimental geometry.

Materials and Methods

ICG and HSA were obtained from Sigma and used without further purification. Concentrations of ICG and HSA were determined using extinction coefficients of ϵ (780 nm) = 130 000 M^{-1} cm^{-1} and ϵ (278) nm = 37 000 M^{-1} cm^{-1}, respectively.

Glass microscope slides were cleaned by immersion in 30% v/v H_2O_2 and 70% v/v H_2SO_4 for 48 h and then washed in distilled H_2O. The glass surfaces were coated with amino groups by soaking the slides in a solution of (3-aminopropyl)-trimethoxysilane (APS) with different percentages APS (v/v), and different immersion times as indicated.

Silver colloids were formed by the reduction of a warmed solution of silver nitrate and sodium citrate. This procedure is reported to yield homogeneously sized colloids near 20−30 nm in diameter.[20−23] The APS treated slides were soaked in the colloid suspension for the times indicated in the text, followed by rinsing with distilled water. Binding the ICG-HSA to the surfaces, whether quartz or silver, was accomplished by soaking both the quartz and colloid coated slides in a 30 μM ICG, 60 μM HSA solution overnight, followed by rinsing with water to remove the unbound material.

The glass or colloid surfaces were examined in a sandwich configuration in which two coated surfaces faced inward toward an approximate 1 μm thick aqueous sample (Figure 2). In each case the slides were fully coated with APS but only half coated with silver colloids. Excitation and observation were by the front-face configuration (Figure 3). Steady-state emission spectra were recorded using a SLM 8000 spectrofluorometer with excitation using a Spectra Physics Tsunami Ti:sapphire laser in the continuous wave (CW, nonpulsed) mode with 200 mW 760 nm output over a spot diameter near 5 mm.

Time-resolved intensity decays were measured using reverse start−stop time-correlated single photon counting (TCSPC). Vertically polarized excitation at ≈760 nm was obtained using a mode-locked argon-ion pump, cavity dumped pyridine 2 dye laser with a 3.77 MHz repetition rate. The instrument response function, determined using the experimental geometry in Figure 3, for silver colloid films, was typically <50 ps fwhm. The emission was selected at the magic angle, 54.7° using a long-pass filter (Edmund Scientific) that cut off wavelengths below 780 nm, with an additional 830 ± 10 nm interference filter. Control measurements with colloid-coated surfaces without ICG-HSA showed that scattered light contributed less than 1% to the signal of ICG-HSA with or without colloids, which is an important control given the high scattering cross section of metal colloids.[36−38]

The intensity decays were analyzed in terms of the multiexponential model,

$$I(t) = \sum_i \alpha_i \exp(-t/\tau_i) \tag{1}$$

where α_i are the amplitudes and τ_i the decay times, $\sum\alpha_i = 1.0$. The fractional contribution of each component to the steady-state intensity is given by

$$f_i = \frac{\alpha_i \tau_i}{\sum_j \alpha_j \tau_j} \tag{2}$$

The mean lifetime of the excited state is given by

$$\bar{\tau} = \sum_i f_i \tau_i \tag{3}$$

and the amplitude-weighted lifetime is given by

$$\langle \tau \rangle = \sum_i \alpha_i \tau_i \tag{4}$$

The values of α_i and τ_i were determined by nonlinear least squares using nonlinear least squares impulse reconvolution with a goodness-of-fit χ_R^2 criterion.

Results and Discussion

Figure 4 (top) shows an absorption spectrum typical of our colloid-coated APS slides. The absorption centered near 430 nm is typical of colloidal silver particles with subwavelength dimensions but not completely at the small particle limit. Figure 4 (bottom) shows a typical AFM image of the silver colloid coated APS coated glass slides. The colloid sizes are typically >50 nm, which is slightly larger than reported previously,[21−23] which may be due to colloid aggregation on the surface. We investigated the effects of these surface-bound colloids on fluorescence. The surfaces were incubated with ICG-HSA to obtain a monolayer surface coating. The emission spectra showed a remarkable 30-fold larger intensity on the surfaces coated with silver colloids (Figure 5). The fluorescence intensi-

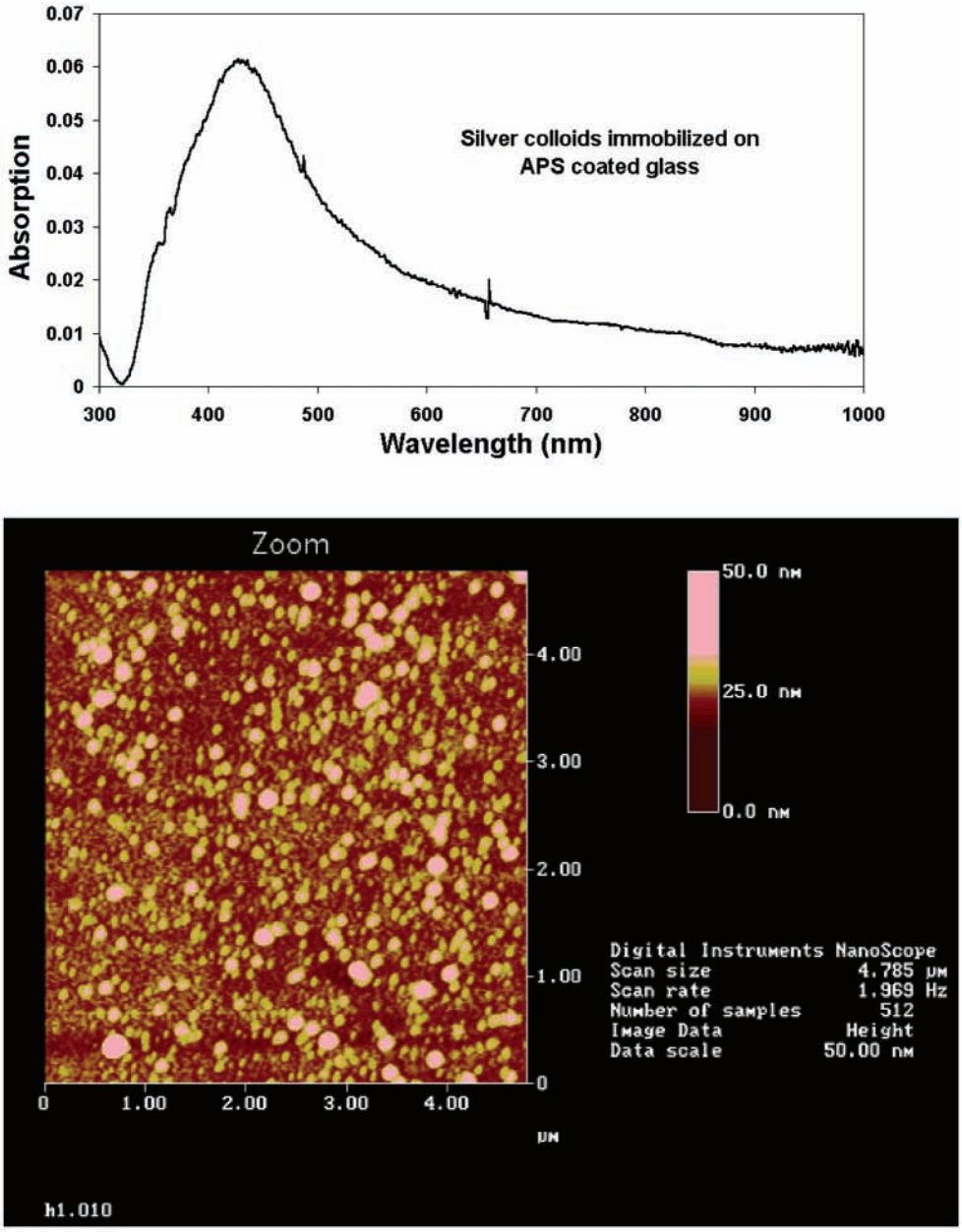

Figure 4. Top: absorption spectrum of silver colloids immobilized on APS coated glass. Bottom: AFM image of a silver colloid coated, 0.5% v/v APS coated glass slide.

ties increased with the concentration of APS used to treat the cleaned surfaces (Figure 6), which also appeared to correlate with the optical density at 430 nm (not shown). It is possible, but unproven, that more colloidal silver is bound when the slides were exposed to higher concentrations of APS.

In general, the enhancement of ICG emission seemed to depend linearly, or at a higher power, on the amount of bound colloids. Theory has predicted that spaces between adjacent colloids may be more effective in increasing fluorescence intensity than isolated colloids.[39] Hence, we expect the ICG intensity to increase *more than linearly* with increasing colloid concentration. The present data do not totally support this expectation, but additional experiments are needed to further clarify whether interacting colloids are superior in enhancing fluorescence.

It is well-known that some fluorophores, particularly those with some conformational freedom, display increased quantum yields in rigid environments. This mechanism seemed unlikely to explain the increased ICG intensity near silver colloids because ICG is bound to the protein, which is then bound to the glass or colloidal surface. Typically, a rigid environment results in decreased rates of nonradiative decay and thus longer lifetimes. In contrast, metallic surface-enhanced fluorescence is expected to result from increases in the rate of radiative decay, which will result in shorter lifetimes.

Time-dependent intensity decays of ICG-HSA were measured when the mixture was in a cuvette (C) and bound to glass (G) or silver colloids (S). The intensity decay is more rapid on glass than in bulk solution in a cuvette, and more rapid when immobilized on silver colloids as compared to on glass (Figure 7, top). At present we do not understand the lifetime reductions on glass, but this effect has been seen for several fluorophores.[11−12] The reduced lifetimes on colloids are due to a rapid 59 ps dominant component in the decay, which can be seen from the fitted parameters (Table 1). The impulse response functions, which are the decays that would be observed with an infinitly short instrument response function (RF), are shown in Figure 7. The contribution of the 59 ps component accounts

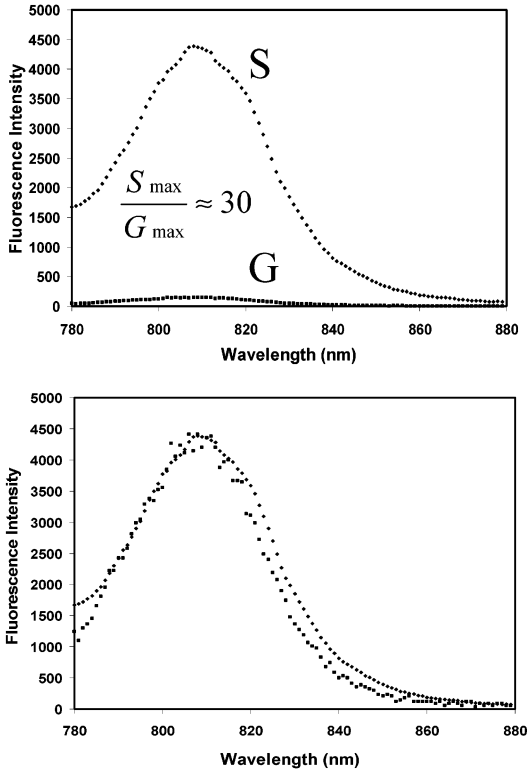

Figure 5. Top: fluorescence intensity of HSA-ICG coated glass, *G*, and above silver colloids, *S*, $E_x = 760$ nm. Bottom: fluorescence intensities normalized to the intensity on silver colloids.

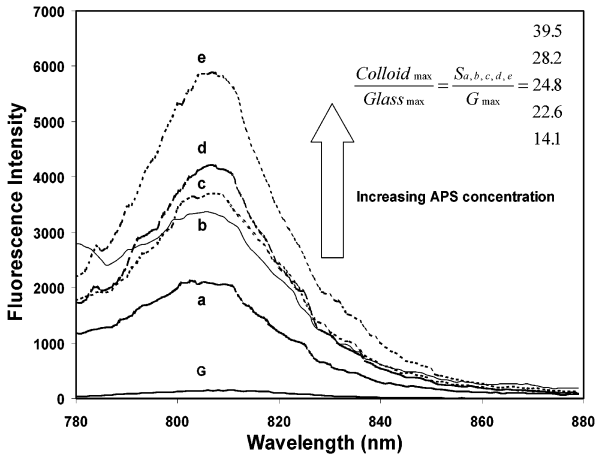

Figure 6. Fluorescence intensity of HSA-ICG on silver colloids as a function of increased [APS] used. Cleaned glass slides were initially soaked in (a) 0.1, (b) 0.25, (c) 0.5, (d) 1.0, and (e) 1.25% (v/v) APS solution for 4 h, washed, and soaked in colloid solution for 4 days. *G* is the fluorescence intensity of HSA-ICG deposited on 0.5% APS covered glass. The ICG coverage for the glass controls, coated with different % APS, was approximately constant.

for 14.7% of the total steady-state ICG intensity and decreases with the amplitude-weighted lifetime from 325 to 68 ps on glass and silver colloids, respectively (Table 1).

We questioned whether the short component in the ICG intensity decay was due to scattered light. Metallic colloids are known to be strongly scattering.[36−38] Control measurements of the glass or colloid-coated slides, without ICG-HSA, yielded a background of much less than 1% when observed through the combination of filters used to isolate the ICG emission. We further examined the possibility of scattered light by recording the emission spectra *through* the emission filter used for the

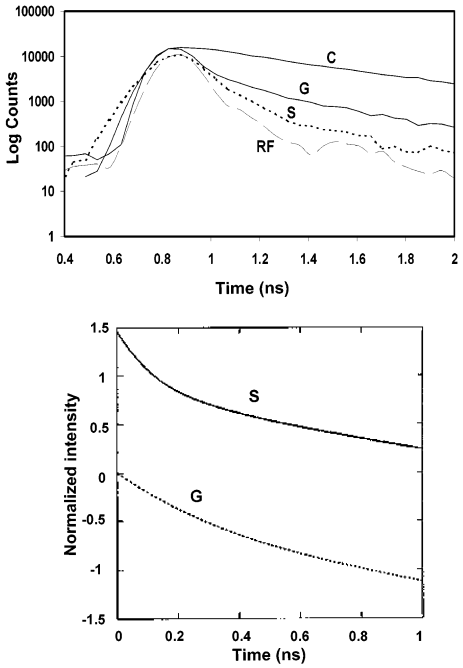

Figure 7. Top: complex intensity decays of ICG-HSA in a cuvette (buffer), C, on glass slides, G, and silver colloids, S. RF is the instrumental response function. Bottom: data from the convolution process normalized to steady-state intensity. I.e., area under S is 39.5 times the area under G (cf. Figure 6).

TABLE 1: Analysis of the Intensity Decay of ICG-HSA Measured Using the Reverse Start−Stop Time-correlated Single Photon Counting Technique and the Multi-exponential Model

sample	α_i	τ_I (ns)	f_i	$\bar{\tau}$ (ns)	$\langle\tau\rangle$ (ns)	χ_R^2
in buffer	0.158	0.190	0.05			
	0.842	0.615	0.95	0.592	0.548	1.4
on quartz	0.683	0.155	0.325			
	0.317	0.691	0.675	0.517	0.325	1.3
on Ag colloids	0.583	0.059	0.147			
	0.211	0.156	0.139			
	0.206	0.817	0.714	0.614	0.068	1.8

time-resolved measurements (Figure 8). These spectra showed no intensity at the excitation wavelength of 760 nm, demonstrating that scattered light is not the origin of the short lifetime components of ICG on colloid-coated slides. However, this was expected as the pulse width of the 760 nm pyridine 2 dye laser was <5 ps. We thus assign the short component to those ICG molecules that have the appropriate proximity and orientation relative to the silver surface to display increased rates of radiative decay. Fluorophores with their transition dipoles oriented parallel to a silver surface are expected to have shorter lifetimes than those with a perpendicular orientation. Because only a fraction of the total emission displays the 59 ps component, and because much of the decay occurs with a lifetime similar to that on glass, it is probable that the 30-fold increase in intensity seen in Figure 5 is due to a subpopulation of the ICG molecules that display greater than 30-fold enhancements.

Another favorable aspect of metal-enhanced fluorescence is the possibility of increased photostability.[10] Photochemical reactions occur while the fluorophores are in the excited state, so one expects that decreased lifetimes should result in an increased photostability. To be more precise, the actual photodecomposition rate may be unchanged, but if the fluorophore returns to the ground state more quickly, there is less time and

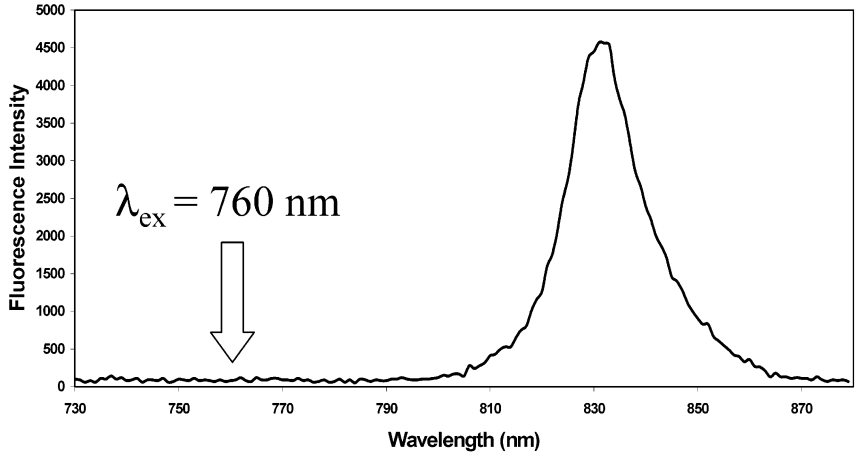

Figure 8. Emission spectrum (magic angle conditions) of ICG-HSA on silver colloids, scanning through the excitation wavelength (vertically polarized 760 nm), using the emission filters used to collect the TD data (i.e., red long-pass filter and a 830 ± 10 nm interference filter).

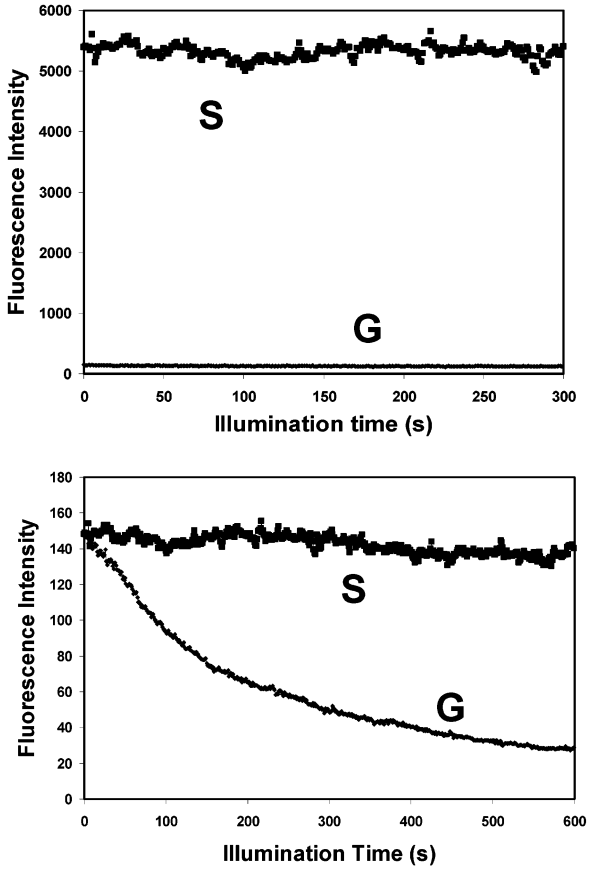

Figure 9. Top: photostability of ICG-HSA on glass and silver colloids, measured using the same excitation power at 760 nm and (bottom) with power *adjusted* to give the same initial fluorescence intensities. In all measurements vertically polarized excitation was used while fluorescence emission was observed at the magic angle, i.e., 54.7°.

therefore a lower possibility, of reactions per excitation de-excitation (emission) cycle.

We examined the photostability of ICG-HSA by recording the steady-state intensity with continuous vertically polarized 760 nm illumination. When illuminated with the same incident intensity (Figure 9, top) the intensity of ICG-HSA on glass or colloids appeared equally photostable. This suggests that the increased intensity seen on the colloids is not due to an increased rate of excitation, which would be expected to result in more rapid photobleaching. We also examined the photostability with the incident light intensities adjusted to result in the same emission intensity (Figure 9, bottom), which in this case is a 30-fold lower incident intensity for the colloid-coated surfaces. Under these conditions ICG-HSA appears to be more photostable on silver than on glass. From the areas under the curves we estimate that each ICG molecule can result in at least 20-fold more detectable signal prior to photobleaching, which could be useful for low copy number assays.

Conclusions and Perspectives

As described in the Introduction, increased intensity from ICG can result in improved imaging to the retinal vasculature. Additional applications can be foreseen for higher intensity ICG probes. One possibility is for use as contrast agent for optical medical tomography. Since the seminal report by Chance and co-workers,[40] there has been intense interest in the use of diffusely scattered red-NIR light for imaging and in vivo physiological monitoring.[41,42] These effects include both steady-state and time-resolved measurements of the scattered light. Although much progress has been made, it is becoming apparent that the contrast in tissues from the red-NIR light is often too small for imaging. As a result there is growing interest in the use of optical contrast agents that remain in the blood vessels or display localized emission due to selective binding or enzymatic activity. The >30-fold increase in ICG intensity found near silver colloids should increase its usefulness for optical contrast in tissues.

The in vivo use of colloids suspensions depends on low or minimal toxicity. We were unable to find publications that describe the toxicity of injected silver colloids directly. However, less direct evidence suggests low toxicity. Colloid silver has been used as an ingestable medicine for over 100 years due to its antimicrobial activity and is still used today to treat or present eye infections in infants. Sublingual silver colloids are thought to appear rapidly in the bloodstream with no reported toxic effects. Lozenges containing silver nitrate are used as an aid to cease smoking.[43,44] It seems probable that some of the silver ions used in this regard become reduced to metallic silver. In addition, silver is in widespread use for sealing dental cavities. The only report of toxicity is for an individual, already ill, who injected silver nitrate antismoking tablets for 40 years.[45] On the basis of this experience and lack of evidence, it seems probable that colloidal silver would be medically safe as an injectable and would thus have a significant impact in optical medical imaging.

Another consideration is the injection of particles (colloids) themselves. Protein-size particles are currently being used in a

variety of medical applications. Liposome and polymers particles are used for drug delivery[46,47] and magnetic particles are being tested for contrast agents for MRI.[48,49] In summary these combined examples suggest the development of dye−colloid conjugates for medical imaging.

Acknowledgment. This work was supported by the NIH National Center for Research Resources, RR-08119.

Abbreviations

APS	(3-aminopropyl)trimethoxysilane
FD	frequency domain
G	APS treated glass slides
HSA	human serum albumin
ICG	indocyanine green
MEF	metal enhanced fluorescence
S	silver colloids on APS treated glass slides
SERS	surface enhanced Raman scattering
SEF	surface enhanced fluorescence
SIFs	silver island films
TCSPC	time-correlated single photon counting
TD	time domain

References and Notes

(1) Henschen, S.; Busse, M. W.; Zisowsky, S.; Panning, B. Determination of plasma volume and total blood volume using indocyanine green: a short review. *J. Medicine* **1993**, *24* (1), 10−27.

(2) Ott, P.; Keiding, S.; Johnsen, A. H.; Bass, L. Hepatic removal of two fractions of indocyanine green after bolus injection in anesthetized pigs. *Am. J. Physiol.* **1994**, *266* (*Gastrointest. Liver Physiol.* 29), G1108.

(3) Still, J. M.; Law, E. J.; Klavuhn, K. G.; Island, T. C.; Holtz, J. Z. Diagnosis of burn depth using laser-induced indocyanine green fluorescence: a preliminary clinical trial. *Burns* **2001**, *27* (4), 364−371.

(4) Sakka, S. G.; Reinhart, K.; Wegscheider, K.; Meier-Hellmann, A. Comparison of cardiac output and circulatory blood volumes by transpulmonary thermo-dye dilution and transcutaneous indocyanine green measurement in critically ill patients. *Chest* **2002**, *121* (2), 559−65.

(5) Schutt, F.; Fischer, J.; Kopitz, J.; Holz, F. G. Indocyanine green angiography in the presence of subretinal or intraretinal haemorrhages: clinical and experimental investigations. *Clin. Exp. Investigations* **2002**, *30* (2), 110−114.

(6) Mueller, A. J.; Freeman, W. R.; Folberg, R.; Bartsch, D.-U.; Scheider, A.; Schaller, U.; Kampik, A. Evaluation of microvascularization pattern visibility in human choroidal melanomas: comparison of confocal fluorescein with indocyanine green angiography. *Graefe's Arch. Clin. Exp. Ophthalmol.* **1999**, *237*, 448−456.

(7) Kramer, M.; Mimouni, K.; Priel, E.; Yassur, Y.; Weinberger, D. Comparison of fluorescein angiography and indocyanine green angiography for imaging of choroidal neovascularization in hemorrhagic age-related macular degeneration. *Am. J. Ophthalmol.* **2000**, *129* (4), 495−500.

(8) Flower, R. W. Experimental studies of indocyanine green dye-enhanced photocoagulation of choroidal neovascularization feeder vessels. *Am. J. Ophthalmol.* **2000**, *129* (4), 501−512.

(9) Flower, R. W.; Von Kerczek, C.; Zhu, L.; Ernest, A.; Eggleton, C.; Topoleski, L. D. T. Theoretical investigation of the role of choriocapillaris blood flow in treatment of subfoveal choroidal neovascularization associated with age-related macular degeneration. *Am. J. Ophthalmol.* **2001**, *132* (1), 85−93.

(10) Lakowicz, J. R. Radiative decay engineering: Biophysical and biomedical applications. *Anal. Biochem.* **2001**, *298*, 1-24.

(11) Lakowicz, J. R.; Shen, Y.; D'Auria, S.; Malicka, J.; Fang, J.; Gryczynski, Z.; Gryczynski, I. Radiative decay engineering 2. Effects of silver island films on fluorescence intensity, lifetimes, and resonance energy transfer. *Anal. Biochem.* **2002**, *301*, 261−277.

(12) Lakowicz, J. R.; Shen, Y.; Gryczynski, Z.; D'Auria, S.; Gryczynski, I. Intrinsic fluorescence from DNA can be enhanced by metallic particles. *Biochem. Biophys. Res. Commun.* **2001**, *286*, 875−879.

(13) Gryczynski, I.; Malicka, J.; Shen, Y.; Gryczynski, Z.; Lakowicz, J. R. Multiphoton excitation of fluorescence near metallic particles: Enhanced and localized excitation. *J. Phys. Chem. B* **2002**, *106*, 2191−2195.

(14) Gersten, J.; Nitzan, A. Spectroscopic properties of molecules interacting with small dielectric particles. *J. Chem. Phys.* **1981**, *75* (3), 1139−1152.

(15) Weitz, D. A.; Garoff, S.; Gersten, J. I.; Nitzan, A. The enhancement of Raman scattering, resonance Raman scattering, and fluorescence from molecules absorbed on a rough silver surface. *J. Chem. Phys.* **1983**, *78*, 5324−5338.

(16) Wokaun, A.; Lutz, H.-P.; King, A. P.; Wild, U. P.; Ernst, R. R. Energy transfer in surface enhanced fluorescence. *J. Chem. Phys.* **1983**, *79* (1), 509−514.

(17) Kneipp, K.; Kneipp, H.; Bhaskaran Kartha, V.; Manoharan, R.; Deinum, G.; Itzkan, I.; Dasari, R. R.; Feld, M. S. Detection and identification of a single DNA base molecule using Surface-Enhanced Raman Scattering (SERS). *Phys. Rev. E* **1998**, *57* (6), R6281-R6284.

(18) Moskovits, M. Surface-enhanced spectroscopy. *Rev. Mod. Phys.* **1985**, *57* (3), 783−826.

(19) Ni, F.; Cotton, T. M. Chemical procedure for preparing surface-enhanced Raman scattering active silver films. *Anal. Chem.* **1986**, *58*, 3159−3163.

(20) Sokolov, K.; Chumanov, G.; Cotton, T. M. Enhancement of molecular fluorescence near the surface of colloidal metal films. *Anal. Chem.* **1998**, *70*, 3898−3905.

(21) Turkevich, J.; Stevenson, P. C.; Hillier, J. A study of the nucleation and growth processes in the synthesis of colloidal gold. *J. Discuss. Faraday Soc.* **1951**, *11*, 55−75.

(22) Henglein, A.; Giersig, Formation of colloidal silver nanoparticles: capping action of citrate. *J. Phys. Chem. B* **1999**, *103*, 9533−9539.

(23) Rivas, L.; Sanchez-Cortes, S.; Garcia-Romez, J. V.; Morcillo, G. Growth of silver colloidal particles obtained by citrate reduction to increase the Raman enhancement factor. *Langmuir* **2001**, *17*, 574−577.

(24) Faraday, M. The Bakerian Lecture. Experimental relations of gold (and other metals) to light. *Philos. Trans.* **1957**, *147*, 145−181.

(25) Kerker, M. The optics of colloidal silver: something old and something new. *J. Colloid Interface Sci.***1985**, *105* (2), 297−314.

(26) Fleischmann, M.; Hendra, P. J.; McQuillan, A. J. Raman spectra of pyridine adsorbed at a silver electrode. *Chem. Phys. Lett.* **1974**, *26* (2), 163−166.

(27) Chen, C. Y.; Burstein, E. Giant Raman scattering by molecules at metal-island films. *Phys. Rev. Lett.* **1980**, *45* (15), 1287−1291.

(28) Vo-Dinh, T. Surface-enhanced Raman spectroscopy using metallic nanostructures. *Trends Anal. Chem.* **1998**, *17* (8−9), 557−582.

(29) Kneipp, K.; Kneipp, H.; Itzkan, I.; Dasari, R. R.; Feld, M. S. Surface-enhanced Raman scattering: A new tool for biomedical spectroscopy. *Curr. Sci.* **1999**, *77* (7), 915−924.

(30) Kummerlen, J.; Leitner, A.; Brunner, H.; Aussenegg, F. R.; Wokaun, A. Enhanced dye fluorescence over silver island films: analysis of the distance dependence. *Mol. Phys.* **1993**, *80* (5), 1031−1046.

(31) Stich, N.; Mayer, C.; Bauer, G.; Schalkhammer, T. DNA biochips based on surface-enhanced fluorescence (SEF) for high-throughput interaction studies. *SPIE* **2001**, *4434*, 128−137.

(32) Schalkhammer, T.; Aussenegg, F. R.; Leitner, A.; Brunner, H.; Hawa, G.; Lobmaier, C.; Pittner, F. Detection of fluorophore-labeled antibodies by surface-enhanced fluorescence on metal nanoislands. *SPIE* **1997**, *2976*, 129−136.

(33) Marchi, M. C.; Bilmes, S. A.; Bilmes, G. B. Photophysics of rhodamine B interacting with silver spheroids. *J. Colloid Interface Sci.* **1999**, *218*, 112−117.

(34) Doron, A.; Katz, E.; Willner, I. Organization of Au colloid as monolayer films onto ITO glass surfaces: Application of the metal colloid films as base interfaces to construct redox-active monolayers. *Langmuir* **1995**, *11*, 1313−1317.

(35) Grabar, K. C.; Freeman, R. G.; Hommer, M. B.; Natan, M. J. Preparation and characterization of Au colloid monolayers. *Anal. Chem.* **1995**, *67*, 735−743.

(36) Yguerabide, J.; Yguerabide, E. E. Light-scattering submicroscopic particles as highly fluorescent analogues and their use as tracer labels in clinical and biological applications, I. Theory. *Anal. Biochem.* **1998**, *262*, 137−156

(37) Yguerabide, J.; Yguerabide, E. E. Light-scattering submicroscopic particles as highly fluorescent analogues and their use as tracer labels in clinical and biological applications, II. Experimental characterization. *Anal. Biochem.* **1998**, *262*, 157−176.

(38) Schultz, S.; Smith, D. R.; Mock, J. J.; Schultz, D. A. Single-target molecule detection with nonbleaching multicolor optical immunolabels. *PNAS* **2000**, *97* (3), 996−1001.

(39) Gersten, J. I.; Nitzan, A. Photophysics and photochemistry near surfaces and small particles. *Surf. Sci.* **1985**, *158*, 165−189.

(40) Ntziachristos, V.; Yodh, A. G.; Schnall, M.; Chance, B. Concurrent MRI and diffuse optical tomography of breast after indocyanine green enhancement. *PNAS* **2000**, *97* (6), 2767−2772.

(41) Sevick-Muraca, E. M.; Lopez, G.; Reynolds, J. S.; Troy, T. L.; Hutchinson, C. L. Fluorescence and absorption contrast mechanisms for

biomedical optical imaging using frequency-domain techniques. *Photochem. Photobiol.* **1997**, *66* (1), 55−64.

(42) Becker, A.; Riefke, B.; Ebert, B.; Sukowski, U.; Rinneberg, H.; Semmier, W.; Licha, K. Macromolecular contrast agents for optical imaging of tumors: Comparison of indotricarbocyanine-labeled human serum albumin and transferrin. *Photochem. Photobiol.* **2000**, *72* (2), 234−241.

(43) Bromberg, L. E.; Braman, V. M.; Rothstein, D. M.; Spacciapoli, P.; O'Connor, S. M.; Nelson, E. J.; Buxton, D. K.; Tonetti, M. S.; Friden, P. M. Sustained release of silver from periodontal wafers for treatment of periodontitis. *J. Controlled Release* **2000**, *68* (1), 63−72.

(44) Lancaster, T.; Stead, L. F. Silver acetate for smoking cessation. *Cochrane Database System Rev.* **2000**, *2*, CD000191.

(45) Ohbo, Y.; Fukuzako, H.; Takeuchi, K.; Takigawa, M. Argyria and convulsive seizures caused by ingestion of silver in a patient with schizophrenia. *Psychiatry Clinical Neurosci.* **1996**, *50* (2), 89−90.

(46) Wang, N.; Wu, X. S. Preparation and characterization of agarose hydrogel nanoparticles for protein and peptide drug delivery. *Pharmaceutical Dev. Technol.* **1997**, *2* (2), 135−142.

(47) Hood, J. D.; Bednarski, M.; Frausto, R.; Guccione, S.; Reisfeld, R. A.; Xiang, R.; Cheresch, D. A. Tumor regression by targeted gene delivery to the neovasculature. *Science* **2002**, *296*, 2404−2407.

(48) Adzamli, K.; Dorshow, R. B.; Hynes, M. R.; Li, D.; Nosco, D. L.; Adams, M. D. Preliminary evaluation of a poly(ethylene glycol)-stabilized manganese-substituted hydroxylapatite as an intravascular contrast agent for MR angiography. *J. Magn. Reson. Imaging* **1997**, *P7* (1), 204−208.

(49) Josephson, L.; Groman, E. V.; Menz, E.; Lewis, J. M.; Bengele, H. A functionalized superparamagnetic iron oxide colloid as a receptor directed MR contrast agent. *J. Magn. Reson. Imaging* **1990**, *8* (5), 637−646.